KAPL-P-000162
(K97043)

CONF-9705305--

MECHANISTIC MODELING OF CHF IN FORCED-CONVECTION SUBCOOLED BOILING

M. Z. Podowski, (S. D'Amico)

May 1997

NOTICE

KAPL ATOMIC POWER LABORATORY SCHENECTADY, NEW YORK 10701

Operated for the U. S. Department of Energy
by KAPL, Inc. a Lockheed Martin company

DISCLAIMER

MECHANISTIC MODELING OF CHF IN FORCED-CONVECTION SUBCOOLED BOILING

Michael Z. Podowski, Ales Alajbegovic, Necdet Kurul, Donald A. Drew and Richard T. Lahey, Jr.
Center for Multiphase Research
Rensselaer Polytechnic Institute
Troy, New York, USA

ABSTRACT

Because of the complexity of phenomena governing boiling heat transfer, the approach to solve practical problems has traditionally been based on experimental correlations rather than mechanistic models. The recent progress in computational fluid dynamics (CFD), combined with improved experimental techniques in two-phase flow and heat transfer, makes the use of rigorous physically-based models a realistic alternative to the current simplistic phenomenological approach. The objective of this paper is to present a new CFD model for critical heat flux (CHF) in low quality (in particular, in subcooled boiling) forced-convection flows in heated channels.

1. BACKGROUND

Numerous experiments have been performed to date to improve our understanding of the subcooled flow boiling and burnout. As summarized below, there are experimental data both focused on the bubble ebullition process, including bubble formation, growth, detachment from the nucleation site, departure from the wall, and collapse, and focused on the conditions which lead to the occurrence of dryout or critical heat flux (CHF).

The processes of bubble formation, its growth/collapse, and flow structure conditions near critical heat flux are shown in Figure 1 and can be classified as:

- Bubble forms at the nucleation site, *i.e.*, an active cavity of a sufficient size (Figure 1, cases I and II).
- The initial growth of a bubble, occurs in the superheated thermal sublayer. This phase is very fast, almost instantaneous, and the bubble has a hemispherical shape (Figure 1, cases I and II)
- After this stage, the top part of the bubble becomes exposed to the subcooled liquid which initiates condensation. At the same time, the bubble may detach from the nucleation site due to the flowing liquid and start sliding along the surface while it is still growing (Figure 1, cases I and II)
- The bubbles can reach their maximum size while being attached to the heated wall (Figure 1, case I). In some situations, the bubbles depart from the surface while they are still growing and reach a maximum size away from (although still relatively close to) the wall (Figure 1, case II). The mechanism which leads to the departure from the wall is not entirely understood. [1,2,3,4,5,6]
- After reaching the maximum size, the bubbles may collapse near the wall (Figure 1, case I[7]) or move away from the wall (Figure 1, case II[8,4,9]). If the subcooling is high and there are many bubbles close together, they will start coalescing and form larger bubbles (Figure 1, case III[10,11,12,13]).
- Finally, large bubbles or slugs almost completely cover the wall surface. Between the large bubbles nucleation of small bubbles may still continue. The length of the large bubbles under these conditions can be estimated by the critical wavelength predicted by Helmholtz instability (Figure 1, case III[13,14]).
- The most important mechanism for the bubble growth is microlayer evaporation.[15,16] Fiori & Bergles[10] performed experiments in boiling water and reported that even at the conditions close to the CHF there was a liquid sublayer beneath the vapor slugs, which was 0.06 mm in thickness. This value is very close to the thickness of the viscous sublayer in turbulent flow under the reported conditions. The conclusion was that those experiments subcooled-boiling CHF did not result from progressive dryout of the sublayer film. Akiyama & Tachiba[17] measured the thickness of the thermal boundary layer and found good agreement when compared with the viscous sublayer thickness. It seems that the bubbles slide on a liquid sublayer whose thickness corresponds to the viscous sublayer. This conclusion is also in agreement with the experimental observations in air/water adiabatic bubbly flow by Moursali et al.[18]

2. MODELING CONCEPT

The physical mechanisms governing subcooled boiling in forced convection, which may eventually lead to CHF accounted for can be described as follows:

At low void factions, the wall heat flux can be partitioned into three major components: single-phase heat convection, evaporation heat flux and heat flux due to quenching (see Fig. 2). The evaporation heat flux is associated with the evaporation in the thin liquid layer beneath the bubbles formed near the wall prior to their departure. The main characteristic of forced-convection subcooled boiling is that it results in very effective heat transfer driven by local evaporation and condensation phenomena under thermodynamic nonequilibrium conditions.

When the number of active nucleation sites increases, and so does the total evaporation rate at the wall, large elongated bubbles start being formed through the effects of coalescence. Consequently, the total wall heat flux can be partitioned into the contribution due to nucleate boiling and the heat transfer rate due to evaporation from the thin liquid sublayer beneath large bubbles formed near the

wall. The heat transfer is severely reduced when the microlayer completely evaporates and is not replenished. This leads to local dryout and wall temperature excursion, the situation known as departure from nucleate boiling (DNB) or critical heat flux (CHF). Since large bubbles slide along the liquid sublayer, their length is important for dryout. Based on existing experimental evidence, bubble length can be approximated by the critical wavelength of the Helmholtz vapor/liquid interface instability. Another possible cause for dryout of the sublayer occurs at high evaporation rates in the nucleate boiling region between large bubbles. The increased bubble concentration possibly combined with interfacial instability (flooding) may effectively prevent replenishment of the liquid near the wall. This effect depends on the size of nucleated bubbles.

The most important effects which lead to dryout and critical heat flux (CHF) can be summarized as:

- dryout of the sublayer beneath large bubbles accumulated along the channel wall, and
- dryout of the sublayer due to prevention of liquid replenishment in the nucleate boiling region.

The most important parameters for the quantification of these effects, are:

- sublayer thickness and evaporation rate,
- the length of large bubbles,
- the evaporation rate in the nucleate boiling region, and
- the bubble diameter on departure from the nucleation site.

An analytical model for the phenomena described above is given in the next section.

3. ANALYTICAL MODEL

For convenience, the overall model has been divided into several parts. The individual partial models are discussed below.

Modes of Wall Heat Transfer in Subcooled Nucleate Boiling

When there is no dryout and in the absence of large bubbles, the wall heat is partially used to form bubbles and the remaining portion is transferred to the liquid. The heat transfer from the wall in the vicinity of a nucleation site occurs during two distinct periods: the bubble growth time and the waiting time. The total convective heat flux from the wall is the sum of three models[19]

$$q''_{conv} = q''_{1\phi} + q''_e + q''_Q \qquad (1)$$

where $q''_{1\phi}$ is the single-phase convective heat flux, q''_e is the heat flux associated with phase change (evaporation), and q''_Q is the so called quenching heat flux, which is transferred to the liquid phase during the waiting time.

Outside of the influence area of the bubbles, the heat transfer from wall to the liquid can be calculated by

$$q''_{1\phi} = A''_{1\phi}\, C_h \rho_l c_{pl} u_l (T_w - T_l) = H_{1\phi}\,(T_w - T_l) \qquad (2)$$

where $A''_{1\phi}$ is the fraction of the wall unaffected by the nucleation sites, C_h is the Stanton number calculated from a heat transfer correlation in terms of the local liquid velocity and Prandtl number, T_w is the wall temperature and T_l is the local liquid temperature near the heated wall. Normally, the wall area affected by a nucleation site is approximately 4 times the projected area of the maximum size of the bubble.[20]

The evaporation heat flux is given by,

$$q''_e = \frac{\pi}{6} d^3_{Bw} \rho_v f n'' h_{fg} \qquad (3)$$

where d_{Bw} is the bubble diameter at detachment, f is the frequency of nucleation, and n'' is the number of nucleation sites per unit area (nucleation site density).

The quenching heat flux has been analytically calculated by Del Valle and Koening[20] as,

$$q''_Q = \tau_w f A''_{2\phi} \frac{2k_l(T_w - T_l)}{\sqrt{\pi \tau_w k_l/(\rho_l c_{pl})}} \qquad (4)$$

where τ_w is the waiting time elapsed between the detachment of a bubble and the nucleation of a subsequent one. The term, $A''_{2\phi}$, is the fraction of the wall area participating in the quenching heat flux.

Formation of Large Bubbles Along the Wall

As it was explained before, when the bubble concentration near the wall increases, the effect of coalescence will result in the formation of large bubbles. Thus, the wall area can be divided into two parts, one associated with nucleate boiling and the other subjected to the large elongated bubbles. This is shown in Figure 3, where the region occupied by large bubbles accounts for two modes of heat transfer: evaporation of the microlayer in Region-I, and heat convection to vapor in Region-II where complete evaporation has occurred. Region-III represents the nucleate boiling mode of heat transfer. Whereas a stationary wall temperature is maintained prior to large bubble formation, the introduction of dry regions where large bubbles touch the wall may cause energy imbalance and, thus, wall temperature fluctuations. The magnitude of these local fluctuations, and the resultant average wall temperature, will depend on the relative effects of the different heat transfer conditions in Regions-I, II and III, as well as on the characteristic passage time for each region.

Let $t_1 - t_0$, $t_2 - t_1$ and $t_3 - t_2$, be the passage times of Regions I, II and III respectively. These time intervals can

be obtained from the known near-wall flow structure. In particular, the relative time of large bubble's passage is

$$\alpha_{wLB} = \frac{t_2 - t_0}{t_3 - t_0} = 1 - \frac{t_3 - t_2}{t_3 - t_0} \tag{5}$$

Also, the dryout time during the large bubble's passage can be related to the overall time of the large bubble passage by introducing a parameter

$$a = \frac{t_2 - t_1}{t_2 - t_0} = 1 - \frac{t_1 - t_0}{t_2 - t_0} \tag{6}$$

By knowing the mean length of large bubbles (or slugs) in the flow direction and their velocity, the following expressions are obtained

$$t_2 - t_0 = \frac{L_{LB}}{v_{LB}} \tag{7}$$

Eqs.(5) and (7) yield

$$t_3 - t_0 = \frac{t_2 - t_0}{\alpha_{wLB}} = \frac{L_{LB}}{\alpha_{wLB} v_{LB}} \tag{8}$$

and

$$t_3 - t_2 = \left(\frac{1 - \alpha_{wLB}}{\alpha_{wLB}}\right)\frac{L_{LB}}{v_{LB}} \tag{9}$$

The interval, t_1-t_0, is the time needed for the complete evaporation of the sublayer beneath the large bubbles, and it can be calculated from

$$t_1 - t_0 = \frac{\delta_0 h_{fg} \rho_l}{q''_w} \tag{10}$$

Naturally, the value obtained from Eq.(10) should not exceed the passage interval of the large bubbles, t_2-t_0.

The length of large bubbles has been measured by Galloway & Mudawar[13] and Gersey & Mudawar[14] and they found it to agree very well with the critical wavelength of the Helmholtz instability vapor/liquid interface. This has been postulated before in the modeling of the large bubble length in subcooled flow boiling.[3,21,22,23] A schematic of the confined wavy liquid-vapor interface is shown in Figure 4.

Stability of a liquid-vapor interface, assuming inviscid, irrotational and two-dimensional flow, has been treated by Lamb[24] and Milne-Thompson.[25] The final result for the pressure difference across the interface is[14]

$$p_l - p_v = -\eta k[\rho''_l (c - v_l)^2 + \rho''_v (c - v_v)^2] + (g \cdot n)\eta(\rho_l - \rho_v) \tag{11}$$

where

$$\rho''_l = \rho_l \coth(k\Delta_l) \tag{12}$$

$$\rho''_v = \rho_v \coth(k\Delta_v) \tag{13}$$

The pressure difference at the interface in the presence of surface tension can be expressed by

$$p_l - p_v = \sigma\kappa = -\sigma\frac{\partial^2 \eta}{\partial x^2}\left[1 + \left(\frac{\partial \eta}{\partial x}\right)^2\right]^{-\frac{3}{2}} \cong -\sigma\frac{\partial^2 \eta}{\partial x^2} \tag{14}$$

The position of the interface with respect to the stationary value can be approximated by the Fourier components of the wave

$$\eta = \eta_0 \exp(ikx + \beta t) \tag{15}$$

Combining Eqs.(14) and (15) yields

$$p_l - p_v = \sigma k^2 \eta \tag{16}$$

Finally, Eqs.(11) and (16) give

$$\sigma k^2 = -k[\rho''_l (c - v_l)^2 + \rho''_v (c - v_v)^2] + (g \cdot n)(\rho_l - \rho_v) \tag{17}$$

Rearranging the above equation yields the following expression for the interfacial velocity

$$c = \frac{\rho''_l v_l + \rho''_v v_v}{(\rho''_l + \rho''_v)} \pm \sqrt{\frac{\sigma k}{(\rho''_l + \rho''_v)} + \frac{(g \cdot n)(\rho_l - \rho_v)}{k(\rho''_l + \rho''_v)} - \frac{\rho''_l \rho''_v (v_v - v_l)^2}{(\rho''_l + \rho''_v)^2}} \tag{18}$$

The critical wavelength is defined as the wavelength that produces a neutrally-stable wave. This wavelength can be calculated by setting the second term in the above equation, which represent the imaginary component of the velocity, equal to zero

$$k_c = \frac{2\pi}{\lambda_c} = \frac{\rho''_l \rho''_v (v_v - v_l)^2}{2\sigma(\rho''_l + \rho''_v)} + \sqrt{\left(\frac{\rho''_l \rho''_v (v_v - v_l)^2}{2\sigma(\rho''_l + \rho''_v)}\right)^2 - \frac{(g \cdot n)(\rho_l - \rho_v)}{\sigma}} \tag{19}$$

In the case where gravity acts in the direction parallel to the mean motion, the critical wavelength becomes

$$k_c = \frac{2\pi}{\lambda_c} = \frac{\rho''_l \rho''_v (v_v - v_l)^2}{\sigma(\rho''_l + \rho''_v)} \tag{20}$$

When the distances between the walls and the liquid/vapor interface, Δ_v and Δ_c, are sufficiently large, the above equation simplifies into the following expression for the critical wavelength

$$k_c = \frac{2\pi}{\lambda_c} = \frac{\rho_l \rho_v (v_v - v_l)^2}{\sigma(\rho_l + \rho_v)} \tag{21}$$

The critical wavelength expressed in Eq.(21) has been used in Refs. 3, 21, 22, 23 for the calculation of large bubbles length. However, in order to make the model applicable to various channel geometries, Eq.(20) is more appropriate, and should be used. Therefore, in this study, the length of a large bubble has been calculated as

$$L_{LB} = \lambda_c = \frac{2\pi\sigma(\rho''_l + \rho''_v)}{\rho''_l \rho''_v (v_v - v_l)^2} \tag{22}$$

Another parameter of interest to the present model is the distance between the elongated bubbles and the wall. As stated before, these bubbles flow very close to the walls, at an initial distance (i.e., at the tip of the bubbles) corresponding to the viscous sublayer thickness.[18] The thickness of the viscous sublayer is specified by

$$y^+ = \frac{u_\tau y}{\nu} = 10 \tag{23}$$

where $u_\tau = \sqrt{\tau_w/\rho_l}$ is the shear velocity. Eq.(23) yields the following expression for the sublayer thickness, d_0,

$$\delta_0 = \frac{10\nu}{u_\tau} \tag{24}$$

Figure 5 shows a schematic of the sublayer beneath a large bubble.

Replenishment of Liquid Sublayer

If the supply of liquid to the sublayer is interrupted, the sublayer cannot be restored after the large bubble's passage. Again, we can use Helmholtz instability to calculate the case when the liquid can no longer replenish the liquid sublayer.

The critical velocity for this case is equal to (see Eq.(21))

$$u_{max} = |u_l - u_g| = \sqrt{\frac{2\pi\sigma(\rho_l + \rho_v)}{\rho_l \rho_v d_{Bw}}} \tag{25}$$

The vapor velocity can be obtained from

$$u_g = \frac{q''_w}{\rho_g h_{fg}} \frac{A_g}{A_w} \tag{26}$$

where A_g/A_w is the fraction of wall area covered by vapor jets. As shown in Fig. 6, the liquid velocity is obtained using the mass conservation,

$$u_l = -u_g \frac{\rho_g}{\rho_l} \frac{A_g}{A_w - A_g} \tag{27}$$

Wall Temperature

The wall temperature as a function of time for each of the regions shown in Figure 3 can be evaluated from the respective energy balances

$$c_{ps}\rho_s L \frac{d}{dt} T_{w,i}(t) = q''_w - q''_{conv,i} \tag{28}$$

for $i=1,2,3$. Solving Eq.(28) for each region yields

$$T_{w1}(t) = T_w(t_0) \tag{29}$$

$$T_{w2}(t) = \tag{30}$$
$$T_w(t_1) Exp\left(\frac{H_v}{c_{ps}\rho_s L_{LB}}(t - t_1)\right) +$$
$$\left(T_{sat} + \frac{q''_w}{H_v}\right)\left[1 - Exp\left(\frac{H_v}{c_{ps}\rho_s L_{LB}}(t - t_1)\right)\right]$$

$$T_{w3}(t) = T_w(t_2) Exp\left(\frac{H_\phi}{c_{ps}\rho_s L_{LB}}(t - t_2)\right) + \tag{31}$$
$$\left(T_l + \frac{q''_{l\phi}}{H_\phi}\right)\left[1 - Exp\left(\frac{H_\phi}{c_{ps}\rho_s L_{LB}}(t - t_2)\right)\right]$$

where ρ_s and c_{ps} are the density and specific heat of the solid wall, and H_v is the vapor heat transfer coefficient.

Taking into account that

$T_{w1}(t_1) = T_{w2}(t_1) = T_w(t_1)$,

$T_{w2}(t_2) = T_{w3}(t_2) = T_w(t_2)$ and

$T_{w3}(t_3) = T_{w1}(t_0) = T_w(t_0)$, and evaluating Eqs.(29), (30) and (31) at t_1, t_2 and t_3, respectively, the resultant system of equations can be solved for

$T_w(t_0) = T_w(t_1)$ and $T_w(t_2)$. Then, Eqs.(29), (30) and (31) can be used to obtain the average wall temperature as

$$\bar{T}_w = \frac{1}{t_3 - t_0} \left[\int_{t_0}^{t_1} T_{w1}(t)dt + \int_{t_1}^{t_2} T_{w2(1)}(t)dt + \int_{t_2}^{t_3} T_{w3}(t)dt \right] \quad (32)$$

Other Closure Relationships

In order to close the present model, additional relationships are needed regarding parameters such as nucleation frequency, nucleations site density, bubble diameter at departure, etc. The closure laws which were originally proposed by Kurul & Podowski are given in Ref. [19]. In addition, the following relations have been used in the present model.

- The bubble diameter can be expressed by

$$d_{Bw} = 0.0014 \exp\left(\frac{\Delta T_{sub}}{45}\right) \quad (33)$$

where ΔT_{sub} is in °C, and d_{Bw} is in m.[26] It is known that the liquid velocity has a significant effect on the bubble diameter at detachment. In order to include the effect of the bubble velocity, a correction was added to Eq.(33) based on the expression given by Unal[27] (also, see Ref. [19]).

The nucleation site density is obtained from the experimental data of Lemmert & Chawla[28]

$$n'' = [m(T_w - T_l)]^{1.805} \quad (34)$$

where $m = 185$.

- The limitation normally imposed on the nucleation site density (i.e., that area of influence cannot overlap) has been relaxed in the present model by assuming that even when the two neighboring nucleation sites are very close to each other, they may still be active if they are nucleating out of phase and if the waiting time is long enough.
- The interfacial heat transfer per unit volume between the bubbles and the liquid in the bulk is given by

$$q'''_i = \frac{k_c}{D_H}\left[2 + 0.6\left(\frac{\rho_c D_d v_r}{\mu_c}\right)^{0.5}\left(\frac{c_{pc}\mu_c}{k_c}\right)^{0.33}\right] A'''_d (T_{sat} - T_l) \quad (35)$$

where A'''_d is the vapor interfacial area density. It has been also assumed that the vapor temperature cannot exceed the saturation temperature and the interfacial phase change (condensation) rate is

$$\Gamma_c = \frac{q'''_i}{h_{fg}} \quad (36)$$

4. RESULTS AND DISCUSSION

The model of subcooled nucleate boiling summarized in Section 3 calculates each of the three modes of wall heat transfer: single-phase convection, quenching and evaporation, as well as the wall temperature. All these parameters are evaluated in terms of the liquid subcooling and velocity in the cell adjacent to the wall. Two typical results are presented in Figures 7 & 8 for water and in Figures 9 & 10 for Freon. The conditions in Figures 9 and 10 are the same as those in the data set of Velindala et al.[29] The heat flux partitioning and predicted wall temperatures at saturation for a range of heat fluxes are shown in Figure 11.

After the formation of large bubbles, the near-wall void fraction is also calculated by the model in addition to the parameters mentioned above. If the actual heat flux is above the critical heat flux at any particular flow and heat transfer conditions, an excursion in the wall temperature would result. This can be illustrated by evaluating the wall temperature for various values of the local near-wall parameters accounted for in the model. In Figs. 12 and 13, the estimated wall temperature is plotted for a range of liquid subcoolings and void fractions for two different liquid velocities for a heat flux of 190 kW/m^2 for Freon. The jump in the wall temperature can be clearly seen at high void fraction and low subcooling indicating that the heat flux in this range is above the critical heat flux. Similar results are shown in Figs. 14 and 15 at two different constant void fractions. As expected, the heat flux is always below the critical heat flux if the void fraction is as low as 0.3 in the next-to-wall node (Fig. 14), while it can be above the critical heat flux at low velocities if the near-wall void fraction is about 0.9 or higher (Fig. 15).

The model predictions have been compared against the experimental data of Hino & Ueda.[30] The test section was a vertical concentric annulus with the inner tube heated. The heated section contained a stainless-steel tube, 8 mm o.d., 400 mm long. The outer tube was made of pyrex tube, 18 mm i.d. The resultant hydraulic diameter was 10 mm. The fluid used in the experiment was Freon R-113 at a fixed pressure of 0.147 MPa (the corresponding saturation temperature was 332 K). The present model was incorporated into the overall model of a boiling channel and numerically implemented using the CFX-4 computer code as a solver of the governing equations.

Tables 1 and 2 give the comparison of the experimental and predicted values of the critical heat flux.

As can be seen, the agreement is better at higher subcooling, the probable cause being that the used nucleate boiling model is more accurate for low subcoolings. Specifically, the bubble nucleation frequency, although calculated from a correlation applicable to a wide range of conditions, apparently overpredicts the evaporation rate at

Table 1: Predicted Critical Heat Fluxes,

$G = 512\ kg/m^2s$

ΔT_{sub} [K]	Measured [30] $[kW/m^2]$	Predicted $[kW/m^2]$	Relative error
30	241	190	-21%
20	211	160	-24%
10	174	125	-28%

Table 2: Predicted Critical Heat Fluxes,

$G = 1239 kg/m^2s$

ΔT_{sub} [K]	Measured [30] $[kW/m^2]$	Predicted $[kW/m^2]$	Relative error
30	332	405	+22%
20	277	302	+9%
10	244	170	-30%

low subcoolings. A sensitivity study showed that adjusting the calculated nucleation frequency within ∓50 % significantly improves the agreement between the predictions and the data. This points to the conclusion that a better model for the nucleation frequency is needed.

5. CONCLUSIONS

Various mechanisms leading to CHF in subcooled boiling have been investigated. As a result of the analysis of various modeling concepts, two major mechanisms have been identified: (1) dryout of the laminar sublayer between the wall and large bubbles, and (2) the flooding-type phenomenon where the increasing bubble nucleation rate in the wall sections not covered by large bubbles prevents the replenishment of liquid at the wall. Both mechanisms have been implemented in such a way that CHF occurs if either condition is satisfied. In order to evaluate the impact of deteriorating boiling/convective heat transfer on the heated wall, a new model has been developed for the wall dynamics. Using the appropriate averaging scheme between the various modes of wall heat removal, this new model evaluates the wall temperature excursion resulting from the imbalance between the rates of heat generation and removal.

The new models have been coupled with the overall boiling channel model, numerically implemented in the CFX 4 computer code, tested and validated against experimental data. In particular, the calculated temperature excursion was compared against the experiments of Hino & Ueda.[30] The predicted critical heat flux for various channel operating conditions shows good agreement with the measurements, using the closure laws stated above for the various local phenomena governing nucleation and bubble departure from the wall. Nevertheless, the observed differences are consistent with typical uncertainties associated with CHF data. [31]

ACKNOWLEDGEMENTS

The authors wish to express their gratitude to: D. Edwards, M. Erdman, C. Gersey and G. Kirouac, for their technical assistance and fruitful technical discussions.

REFERENCES

[1] R.A.M. Al-Hayes and R.H.S. Winterton, "Bubble Growth in Flowing Liquids," *Int. J. Heat Mass Transfer*, Vol. **24**, 213-222, 1981a.

[2] R.A.M. Al-Hayes and R.H.S. Winterton, "Bubble Diameter on Detachment in Flowing Liquids," *Int. J. Heat Mass Transfer*, Vol. 24, 223-230, 1981b.

[3] Y. Haramura and Y. Katto, "A New Hydrodynamic Model of Critical Heat Flux, Applicable Widely to Both Pool and Forced Convection Boiling on Submerged Bodies in Saturated Liquids," *Int. J. Heat Mass Transfer*, **26**, 389-399, 1983.

[4] J.F. Klausner, R. Mei., D.M. Bernhard and L.Z. Zeng, "Vapor Bubble Departure in Forced Convection Boiling," *Int. J. Heat Mass Transfer*, **36**, 651-662, 1993.

[5] S.G. Kandlikar and B.J. Stumm, "A Control Volume Approach for Investigating Forces on a Departing Bubble Under Subcooled Flow Boiling," *4th Thermophysics and Heat Transfer Conference*, Colorado Springs, HDT-Vol.273, 73-80, 1994.

[6] W.G.J. van Helden, C.W.M. Van Der Geld and P.G.M. Boot, "Forces on Bubbles Growing and Detaching in Flow Along Vertical Wall," *Int. J. Heat Mass Transfer*, **38**, 2075-2088, 1995.

[7] F.C. Gunther, "Photographic Study of Surface-Boiling Heat Transfer to Water With Forced Convection," *ASME Transactions*, **73**, 115-123, 1951.

[8] A.H. Abdelmessih, F.C. Hooper and S. Nangia, "Flow Effects and Bubble-Growth and Collapse in Surface Boiling," *Int. J. Heat Mass Transfer*, Vol. 15, 115-125, 1972.

[9] E.L. Bibeau and M. Salcudean, "A Study of Bubble Ebullition in Forced-Convective Subcooled Nucleate Boiling at Low Pressure," *Int. J. Heat Mass Transfer*, **37**, 2245-2259, 1994.

[10] M.P. Fiori and A.E. Bergles, "Model of Critical Heat Flux in Subcooled Flow Boiling," *4th International Heat Transfer Conference*, Paris, Vol.6, B6.3, 1970.

[11] S.B. van der Molen and F.W.B.M. Galjee, "The Boiling Mechanism During Burnout Phenomena in Subcooled Two-Phase Water Flows," *Vi International Heat Transfer Conference*, Vol. 1, 381-385, 1978.

[12] V.H. Del Valle M., "An Experimental Study of Critical Heat Flux in Subcooled Flow Boiling at Low Pressure Including The Effect of Wall Thickness," *ASME-JSME Thermal Engineering Joint Conference*, Honolulu, Vol. 1, 143-150, 1983.

[13] J.E. Galloway and I. Mudawar, "CHF Mechanism in Flow Boiling From a Short Heated Wall-I. Examination

of Near-Wall Conditions With the Aid of Photomicrography and High-Speed Video Imaging," *Int. J. Heat Mass Transfer*, **36**, 2511-2526, 1993.

[14] C.O. Gersey and I. Mudawar, "Effects of Heater Length and Orientation on the Trigger Mechanism for Near-Saturated Flow Boiling Critical Heat Flux- I. Photographic Study and Statistical Characterization of the Near-Wall Interfacial Features," *Int. J. Heat Mass Transfer*, **36**, 629-641, 1995.

[15] M.G. Cooper and A.J.P. Lloyd, "The Microlayer in Nucleate Pool Boiling," *Int. J. Heat Mass Transfer*, **12**, 895-913, 1969.

[16] M.G. Cooper, K. Mori and C.R. Stone, "Behavior of Vapor Bubbles Growing at a Wall With Forced Flow," *Int. J. Heat Mass Transfer*, **26**, 1489-1507, 1983.

[17] M. Akiyama and F. Tachiba, "Motion of Vapor Bubbles in Subcooled Heated Channel," *Bulletin of the JSME*, **17**, 241-247, 1974.

[18] E. Moursali, J.L. Marie, and J. Bataille, "An Upward Bubbly Boundary Layer Along a Vertical Flat Plate," *Int. J. Multiphase Flow*, **21**, 107-117, 1995.

[19] N. Kurul and M.Z. Podowski, "On The Modeling of Multidimensional Effects in Boiling Channels," ANS Proc. 27th National Heat Transfer Conference, Minneapolis, MN, July 28-31, 1991.

[20] M. Del Valle and D.B.R. Koening, "Subcooled Flow Boiling at High Heat Flux," *Int J. Heat Mass Transfer*, Vol. 28, pp. 1907-1920 (1985).

[21] C.H. Lee and I. Mudawar, "A Mechanistic Critical Heat Flux Model for Subcooled Flow Boiling Based on Local Bulk Flow Conditions," *Int. J. Multiphase Flow*, **14**, 711-728, 1988.

[22] Y. Katto, "A Physical Approach to Critical Heat Flux of Subcooled Flow Boiling in Round Tubes," *Int. J. Heat Mass Transfer*, **33**, 611-620, 1990.

[23] G.P. Celata, M. Cumo, A. Mariani, M. Simoncini and G. Zummo, "Rationalization of Existing Mechanistic Models for the Prediction of Water Subcooled Flow Boiling Critical Heat Flux," *Int. J. Heat Mass Transfer*, **37**, 347-360, 1994.

[24] H. Lamb, *Hydrodynamics*, Dover, New York, 1945.

[25] L.M. Milne-Thompson, *Theoretical Hydrodynamics*, Macmillan, New York, 1960.

[26] V.I. Tolubinsky and D.M. Kostanchuk, "Vapour Bubbles Growth Rate and Heat Transfer Intensity at Subcooled Water Boiling," *Proc. 4th International Heat Transfer Conference*, Vol. 5, Paper No. B-2.8, Paris, France, (1970).

[27] H.C. Unal, "Maximum Bubble Diameter, Maximum Bubble Growth Time and Bubble Growth Rate During Subccoled Nucleate Flow Boiling of Water up to 17.7 MW/m^2," *Int. J. Heat Mass Transfer*, Vol. 19, pp. 643-686, (1976).

[28] M. Lemmert and J.M. Chawla, "Influence of Flow Velocity on Surface Boiling Heat Transfer Coefficient," *Heat Transfer in Boiling*, Ed. E.Hahne and U. Grigull, Academic Press and Hemisphere (1977).

[29] V. Velindala, S. Putta, R.P. Roy and S.P. Kaira, "Velocity Field in Turbulent Subcooled Boiling Flow," HTD-Vol. 314, ASME Proc. of 30th National Heat Transfer Conference, Portland, Oregon (1995).

[30] R. Hino, T. Ueda, "Studies on Heat Transfer and Flow Characteristics in Subcooled Flow Boiling-Part 2. Flow Characteristics," *Int. J. Multiphase Flow*, **11**, 283-397, 1985.

[31] N.E. Todreas and M.S Kazimi, *Nuclear Systems I - Thermal Hydraulic Fundamentals*, Hemisphere Publishing Corp., 1991.

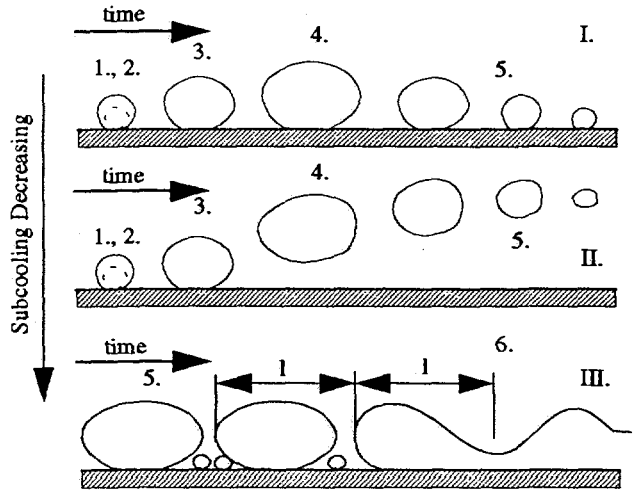

Figure 1. Vapor structures close to the heated wall in the subcooled flow boiling.

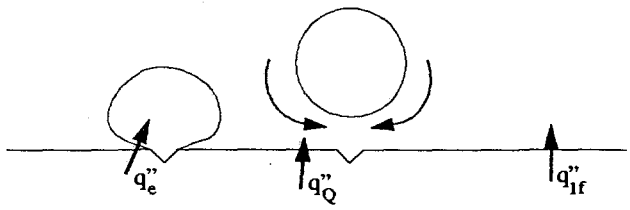

Figure 2. Vapor structures close to the heated wall in the subcooled flow boiling.

I. sublayer evaporation in slugs (large bubbles)
II. convection to vapor (dryout)
III. convection to liquid and nucleate boiling

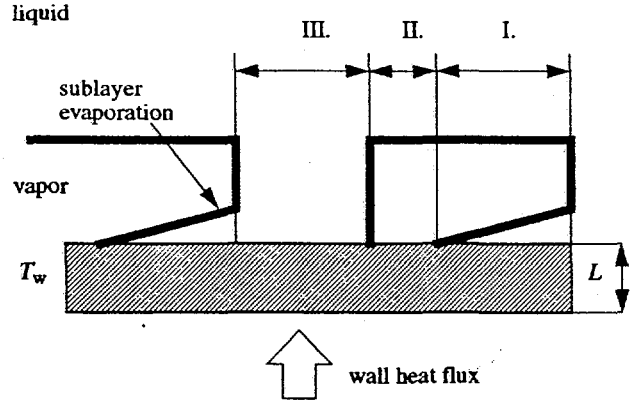

Figure 3. A schematic of structures important for the wall heat partitioning.

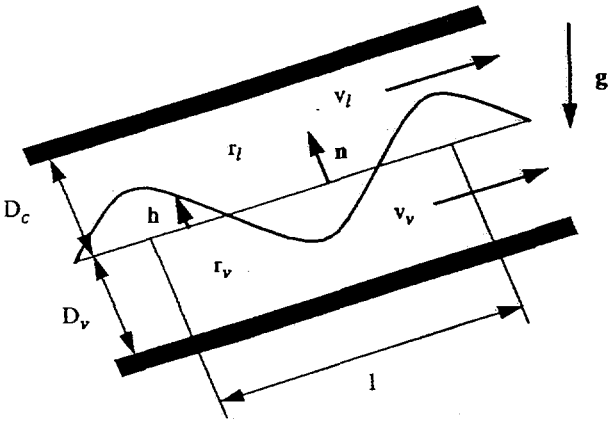

Figure 4. Confined two-dimensional wavy liquid-vapor interface.

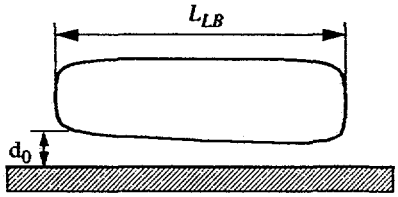

Figure 5. Schematic representation of the film thickness beneath the sliding vapor bubbles.

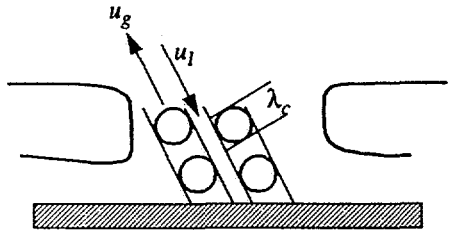

Figure 6. Schematic representation of the physics used in the calculation of the limit of liquid resupply to the sublayer.

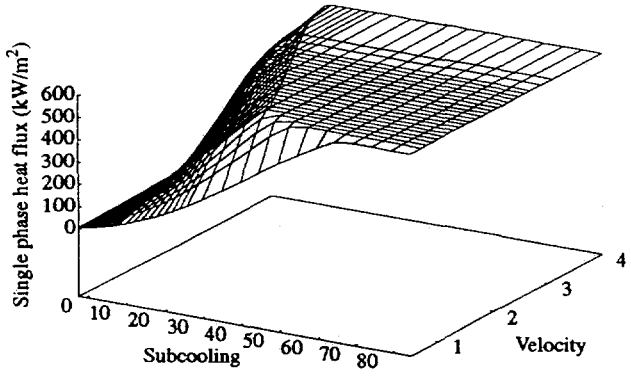

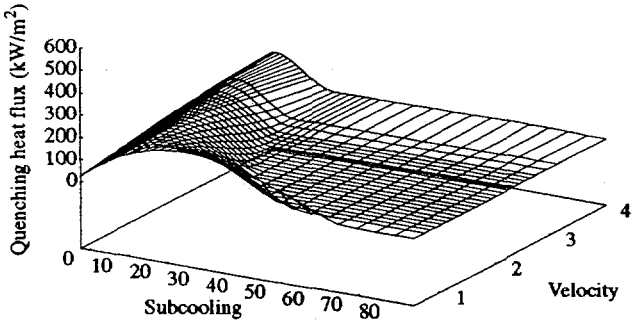

Figure 7. Heat flux partitioning and wall temperature for water at p = 45 bars, q'' = 600 kW/m^2

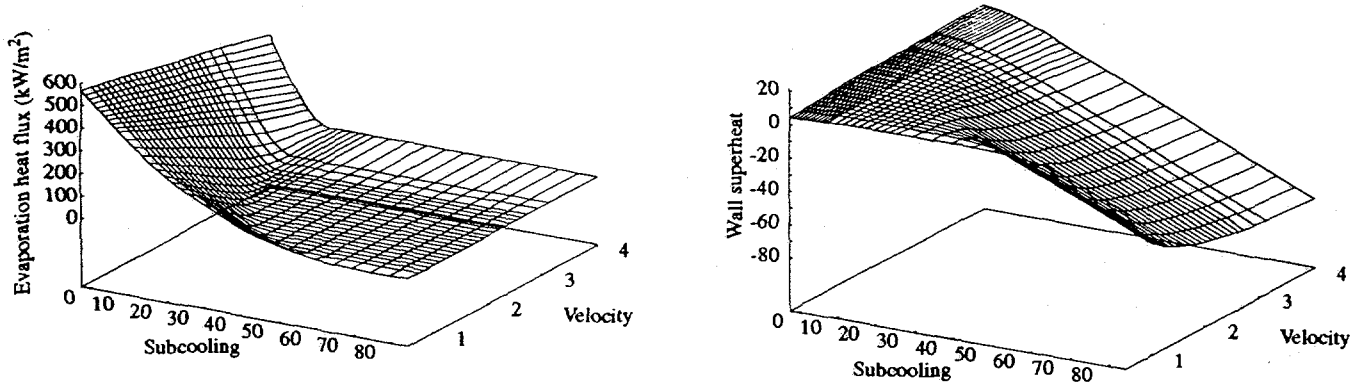

Figure 8. Heat flux partitioning and wall temperature for water at p = 45 bars, q'' = 600 kW/m^2

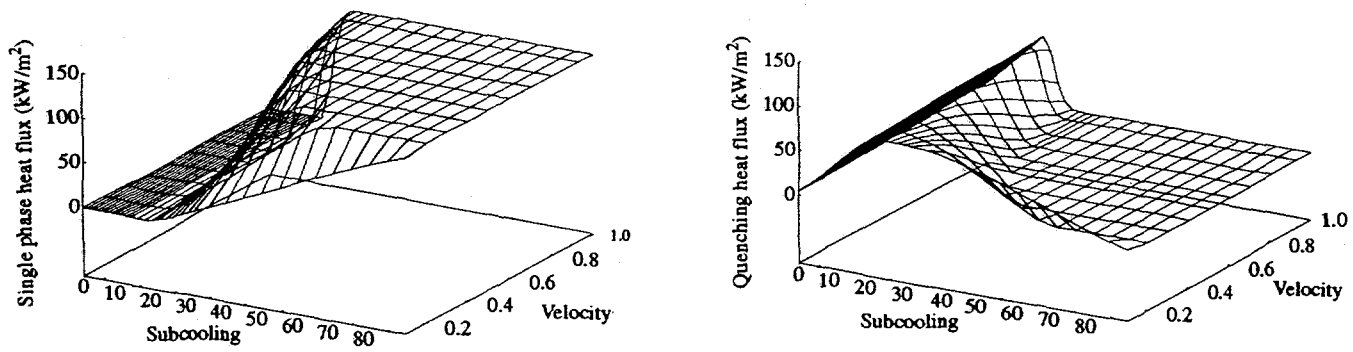

Figure 9. Heat flux partitioning and wall temperature for Freon at p = 2.77 bars, q'' = 125 kW/m^2 (continued on next page)

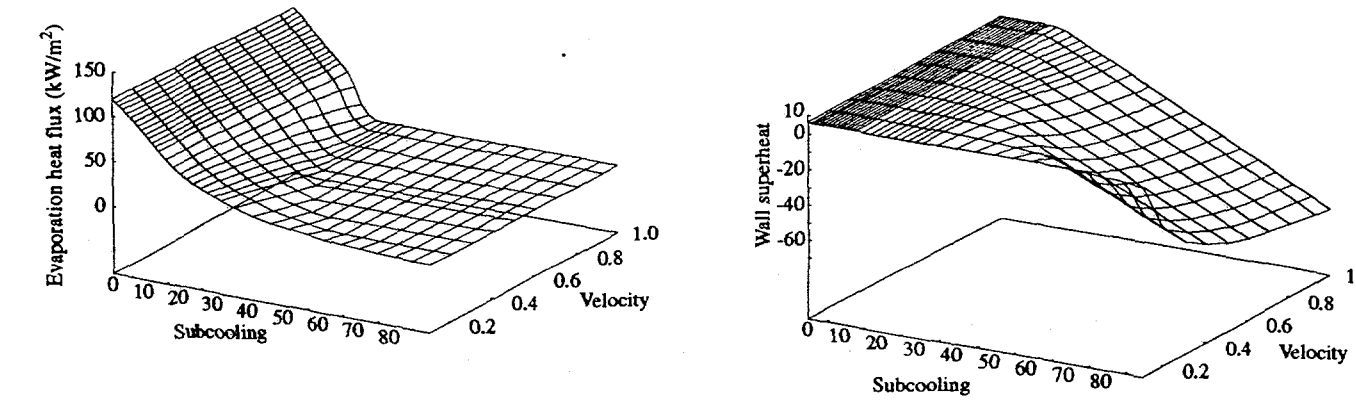

Figure 10. Heat flux partitioning and wall temperature for Freon at p = 2.77 bars, q'' = 125 kW/m^2 (continued from previous page)

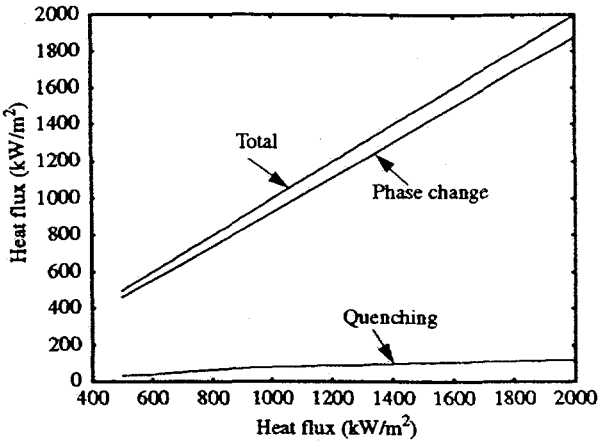

Figure 11. Heat flux partitioning for saturated conditions for water at 45 bars. Liquid velocity: 0.1 m/s

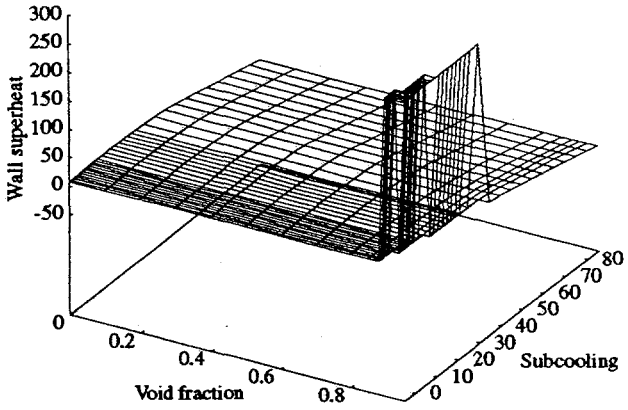

Figure 12. Critical heat flux, Freon at p = 1.5 bars, q"=190 kW/m^2 at constant liquid velocity of 0.5 m/s

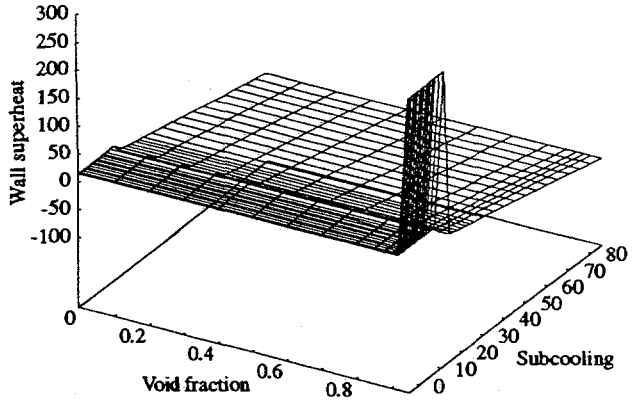

Figure 13. Critical heat flux, Freon at p = 1.5 bars, q"=190 W/m^2 at constant liquid velocity of 2.0 m/s

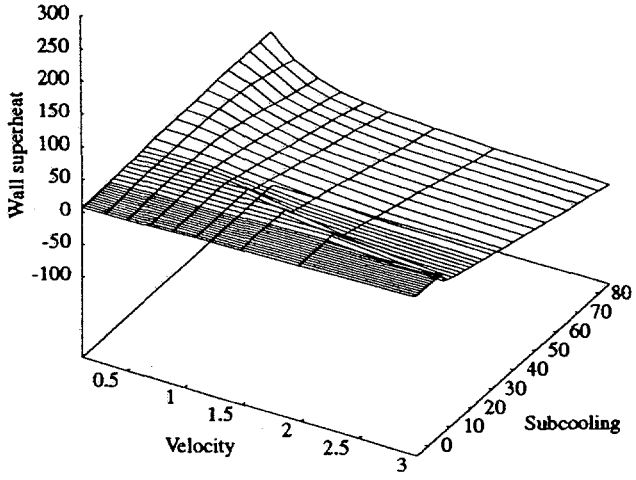

Figure 14. Critical heat flux, Freon at p = 1.5 bars, q"=190 kW/m^2 at constant void fraction of 0.3

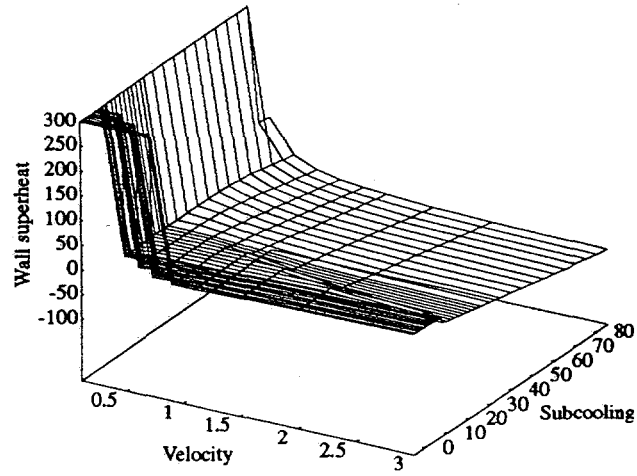

Figure 15. Critical heat flux, Freon at p = 1.5 bars, q"=190 kW/m^2 at constant void fraction of 0.9